

SLOVAK UNIVERSITY OF TECHNOLOGY  
IN BRATISLAVA

FACULTY OF ELECTRICAL ENGINEERING  
AND INFORMATION TECHNOLOGY



**Electromagnetic and Electrothermal modeling  
of superconductors  
for large scale applications**

**Summary of doctoral dissertation**

**Anang Dadhich**

A dissertation submitted for the degree of  
Philosophiae Doctor in doctoral study programme:  
**5.2.48 Physical Engineering**

**Bratislava 2021**

This thesis was developed in a full-time doctoral study at Institute of Electrical Engineering, Department of Superconductors, Slovak Academy of Sciences in Bratislava.

Author: **MSc. Anang Dadhich**

Institute of Electrical Engineering SAS  
Dúbravská cesta 9,  
841 04 Bratislava

Supervisor: **Mgr. Enric Pardo, PhD**

Institute of Electrical Engineering SAS  
Dúbravská cesta 9,  
841 04 Bratislava

Opponents: **prof. Ing. Pavol Rafajdus, PhD**

Žilina University in Žilina  
Univerzitná 8215/1,  
010 26 Žilina

**Dr. Philippe Vanderbenden**

University of Liege  
Quartier Polytech 1, allée de la Découverte 10, 4000 Liège 1  
Belgique

Dissertation thesis abstract was sent:

Dissertation Thesis defence will be held on:

Dean of the faculty FEI, STU: prof. Dr. Ing. Miloš Oravec

# Contents

<b>1</b>	<b>Introduction</b>	<b>2</b>
<b>2</b>	<b>Modeling method</b>	<b>4</b>
<b>3</b>	<b>Cross field demagnetization of HTS stacks</b>	<b>7</b>
3.1	Instantaneous dependence of trapped field . . . . .	7
3.2	Dynamic Magneto-Resistance approach . . . . .	11
3.2.1	Demagnetization of 100 tape stack for millions of cycles . . . . .	14
3.3	Other configurations . . . . .	16
<b>4</b>	<b>Coupled Electro-Magnetic and Electro-Thermal model</b>	<b>19</b>
4.1	Quench modeling with voltage input . . . . .	19
4.2	Quench modeling with applied field input . . . . .	21
<b>5</b>	<b>Conclusion</b>	<b>27</b>

# Chapter 1

## Introduction

High Temperature Superconducting (HTS) stacks of tapes and bulks can be used as strong permanent magnets in the rotors of hybrid-electric fully superconducting motors for Hybrid Distributed Electric Propulsion in aviation [1]. The major issue with such superconducting motors, though, is the high rate of cross-field demagnetization of HTS tapes present in the rotor of the motor due to stray ripple magnetic fields from motor background/surroundings. This makes the superconductor lose its trapped field, and hence the magnetization (Figure 1.1), thus, causing the premature stopping of motor [2–5]. The numerical analysis methods and commercial software used for the computation of electromagnetic state variables in this phenomenon are quite slow and limited, and, thus, a better program to model the cross field demagnetization of superconductors is required to model a practical case of the superconducting motors in HDEP systems in hybrid electric aircraft, that requires calculations for millions of ripple field cycles [3, 4, 6–12].

Thus, it is the goal of this PhD to develop a 2D computer program, in C++ using E-J Power Law (called Power Law model), capable of modeling cross-field demagnetization in stacks (of very wide and thin tapes), and bulks for realistic motors. Semi-empirical formulas for demagnetization decay time constant are to be realized for HTS stacks of tapes. As the superconducting motors for aviation operate at very high frequencies (in the range of 1000s of Hz), we have also developed a new effective E-J relation (called DMR model), which is able to calculate the demagnetization of very thick superconducting stacks (up to 100 tapes) for millions of cycles of applied cross field.

Also, a major problem that the superconducting coils in high field magnets and electrical applications (like motor, generators, reactors, accelerators, etc.) face is the electro-magneto-thermal quench, which can drive the superconductor material into its ‘normal’ state, where all the benefits of superconductivity cease to exist [13, 14]. Thus, it is essential to model the quench behavior in the designing of superconducting magnets under different local electro-thermal conditions, as the quenching effect is able to rapidly destroy the superconducting magnets. There are numerous software that can model the Electro-Magnetic and Electro-Thermal behavior of superconductors, for magnetic quench and other phenomenon, but there is a need for a simple and fast software that can perform ‘cou-

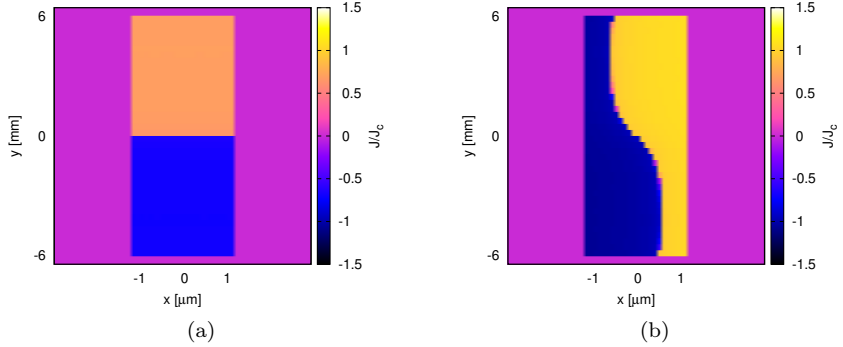


Figure 1.1: Current density distribution (a) after Field-Cool magnetization (applied field parallel to  $x$ - axis), and (b) after 30 cycles of cross magnetic field (ripple field parallel to  $y$ - axis), calculated by our numerical method for 1 tape of  $2 \mu\text{m}$  thickness with power law exponent as 30.

pled' Electro-Magnetic and Electro-Thermal analysis of superconductors quickly and accurately. Thus, another goal of the proposed thesis is to develop a simple and an effective software in C++, using original in-house methods (MEMEP and METEP), that can analyze the coupled Electro-Magnetic and Electro-Thermal behavior of superconductor under different inputs such as applied voltage and applied magnetic field.

# Chapter 2

## Modeling method

We use Minimum Electro-Magnetic Entropy Production (2D MEMEP) method in this PhD to solve for current density,  $J$ , in Electro-Magnetic (EM) model [15–17].

The time constant ( $\tau$ ) can be understood as the time that it takes for the superconducting stack to reach  $1/e$  of its original magnetization (around 37 percent), with  $e$  being the Euler number, since the application of ripple field or the start of demagnetization procedure. The approximated formulas of time constant for a single tape, thin stack of tapes, and thick stack of tapes, respectively, found analytically during this thesis work using uniform  $J$ , are

$$\frac{1}{\tau} = \frac{f\pi}{\ln 2} \frac{d}{w} \left( \frac{B_m}{B_p} - 1 \right), \quad (2.1)$$

$$\frac{1}{\tau} = \frac{f\pi}{\ln 2} \frac{d}{wn} \left( \frac{B_m}{B_p} - 1 \right), \quad (2.2)$$

and

$$\frac{1}{\tau} = \frac{3}{2} f \frac{dh}{w^2 n} \left( \frac{B_m}{B_p} - 1 \right), \quad (2.3)$$

where,  $w$ ,  $d$ ,  $B_p$  are the width, thickness, and parallel penetration field of the tape respectively,  $f$  and  $B_m$  are the applied ripple field frequency and amplitude respectively,  $n$  and  $h$  are the number of tapes in stack and total height of stack respectively, and the critical current density,  $J_c$ , is assumed to be constant. We compare our formula with Brandt's formula for single tape (uses non-uniform  $J$ ), and results from our numerical method.

We have also developed an effective  $E(J)$  relation, which is used in 2D MEMEP model, in place of E-J Power Law, to calculate demagnetization of superconducting stacks for millions of cycles. For effective constitutive model based on dynamic magneto-resistance (DMR), we can divide a thin film superconductor into elements across the width, with each element having tape thickness (Figure 2.1(b), right). Then these elements can each be treated as individual slabs, given their high aspect ratios and negligible mutual magnetic shielding effects of the magnetic field's parallel component [2]. The derived effective  $E(J)$  relation is

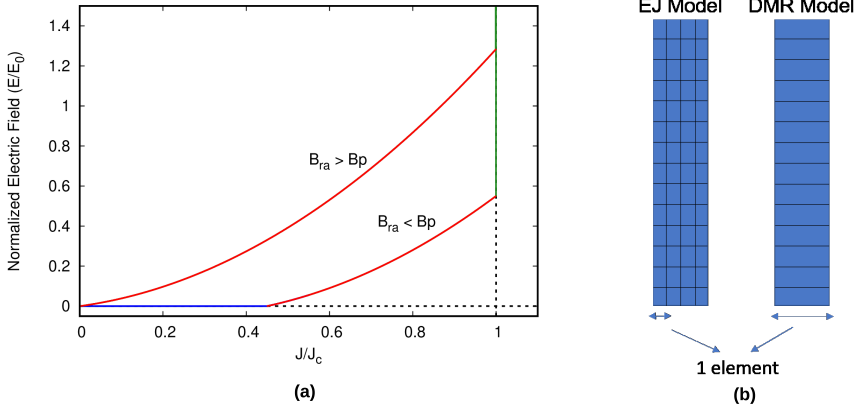


Figure 2.1: (a) The  $E(J)$  relation derived from the dynamic-magneto-resistance (DMR) model. (b) shows that the DMR model require only 1 element in thickness mesh for the tape which makes the calculations faster.

$$E(J) = \begin{cases} 0, & \text{if } B_{ra} \leq B_{th}(J) \text{ and } |J| < J_c, \\ E_R(J), & \text{if } B_{ra} \geq B_{th}(J) \text{ and } |J| < J_c, \\ \rho(|J| - J_c) \frac{J}{|J|} + E_R(J = J_c), & \text{if } |J| \geq J_c, \end{cases} \quad (2.4)$$

where, electric field due to DMR,  $E_R(J)$ , is

$$E_R(J) = E_0 \left[ \frac{B_{ra}}{B_p} - \frac{B_{th}}{B_p} \left( \frac{J}{J_c} \right) \right] \frac{J}{J_c}, \quad (2.5)$$

and threshold magnetic field ( $B_{th}$ ) being

$$B_{th} \left( \frac{J}{J_c} \right) = B_p \left( 1 - \left| \frac{J}{J_c} \right| \right). \quad (2.6)$$

From Figure 2.1(a), it can be seen that there is no DMR when applied ripple field,  $B_{ra}$ , is less than  $B_{th}(J)$ , and hence  $E$  vanishes. Also, when  $B_{ra}$  is above  $B_p$ , there exists a non-zero  $E$  for any non-zero  $J$ .

Similarly, to solve for temperature in superconductors, an original variational principle method- Minimum Electro-Thermal Entropy Production

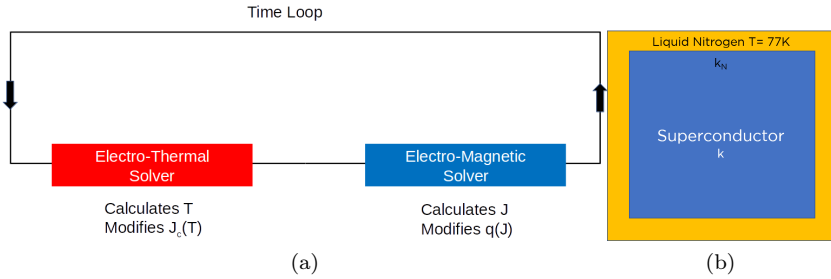


Figure 2.2: (a) Schematic of the coupling process of ElectroMagnetic and ElectroThermal solver.(b) Sketch of the considered square superconducting bulk sample for the thesis.

(METEP) is used. The MEMEP and METEP models are coupled with each other in a single solver, to perform an overall analysis of Electro-Magnetic and Electro-Thermal properties of superconducting sample on the application of external magnetic field or current, or both. Both MEMEP and METEP solvers are connected through a time loop, where METEP is solved first and then MEMEP is solved, for each time step for number of cycles, as can be seen in Figure 2.2 (a).

In this solver, the critical current density  $J_c$  is not constant, and depends on temperature. For superconductors in contact with liquid Nitrogen, a strongly non-linear convection at the boundary exists (as we consider in this thesis- Figure 2.2 (b)), which leads to a boiling heat transfer. In the initial stages of this coupled software development, we have considered a constant physical conductivity parameter,  $k_N$  for the surfaces in contact with liquid Nitrogen, from the convection coefficient for nucleate boiling phase,  $h$ , obtained from [18].

# Chapter 3

## Cross field demagnetization of HTS stacks

Magnetization trends in superconducting tapes have been analyzed in this section, depending on different parameters. The thickness of the tape considered is  $2 \mu\text{m}$ , unless otherwise specified, and the separation between tapes is  $60 \mu\text{m}$  for the stacks of tapes. The sample is first magnetized through Field Cooling process for 100 seconds, 300 mT applied field magnitude, and later it is set to be relaxed for 900 seconds. After relaxation, a demagnetizing ripple field is applied in transverse direction with high frequency of 500 Hz and peak ripple field amplitudes ranging from 2 mT to 200 mT (Figure 3.1). The trapped field is calculated at an observation point located at 1 mm distance from the center of the tape in the  $x$  direction for single tapes (Figure 3.1).

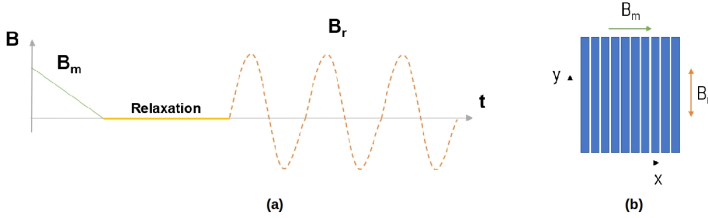


Figure 3.1: (a) Field is applied firstly for magnetization, then after relaxation tranverse alternating field is applied to check demagnetization. (b) shows the directions for magnetizing( $B_m$ ) and ripple cross fields ( $B_r$ ).

## Instantaneous dependence of trapped field

### Benchmark of 2D MEMEP model with 3D MEMEP model

The 2D MEMEP model being used in this document is benchmarked with the 3D MEMEP model from [16]. All the parameters for this calculation are same, except that the 3D model uses a superconducting tape with a finite length, and the 2D model is applied to an infinitely long tape. Figure 3.2 (a) and (b), shows very good agreement between both models, and specially when the tape length is 3 times or more the width, 2D

MEMEP can be used accurately, as the results are practically same for long samples.

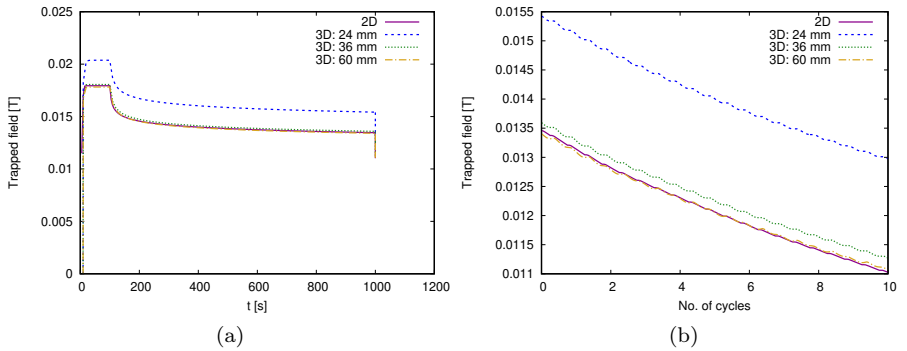


Figure 3.2: Benchmark of 2D MEMEP model with 3D MEMEP model for (a) the whole trapped field curve, and (b) the demagnetization phase. 2D model is realistic for long samples.

## Current density

The current density profiles for a stack of 10 tapes, with each tape of thickness  $2 \mu\text{m}$  and width 12 mm, and applied ripple field of 200 mT for 30 cycles, can be seen in Figure 3.3. By the end of magnetization and relaxation phase, we see the stack is fully penetrated and saturated (Figure 3.3 (a)). On application of cross ripple field, we see some penetration of opposing currents in the sample, which is an indication of demagnetization of sample (Figure 3.3 (b)). The demagnetization of a single tape can be seen in Figure 1.1. Comparing the stack with a single tape in the above figures shows that a single tape has more penetration of opposing screening currents in the sample for the same amount of cycles.

## Dependence on state variables

For this calculation, constant  $J_c d$  or constant sheet current is considered. From Figure 3.4 (a), it can be seen that the demagnetization percentage and rate increases with increase in thickness. Thus, a strong thickness dependence is observed here and we show that artificial thickness should

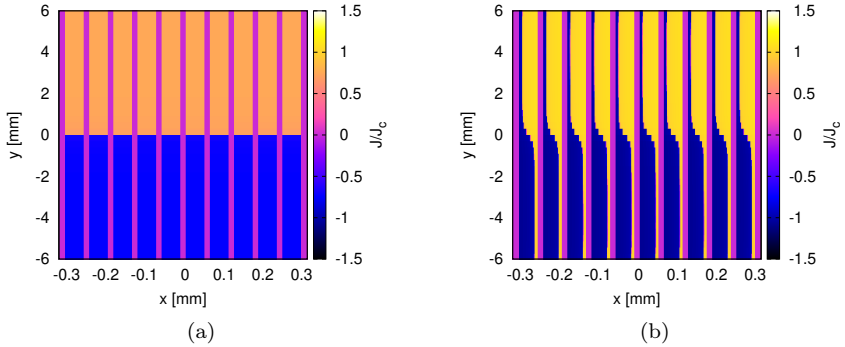


Figure 3.3: Current density profiles for the 10 - tape stack (a) after Relaxation, and (b) demagnetization from application of 30 cross field cycles.

be avoided in modeling the demagnetization of HTS stacks. It can also be seen here that the demagnetization increases with cross field amplitude. There is almost negligible change at low fields. Similarly, there is less demagnetization for higher number of tapes in a stack (Figure 3.4 (b)), and thicker stacks should be considered for solving this problem of cross field demagnetization.

### Time constant study

A comprehensive time constant study has been carried out to check the rate of demagnetization of superconducting tapes, and its dependence on various parameters such as tape thickness and width, applied ripple field amplitude and frequency, and number of tapes in a superconducting stack. All cases that are considered here are for  $2 \mu\text{m}$  tape with critical current density of  $1.36 \times 10^{10} \text{ A/m}^2$ , and 200 mT of applied ripple field with 500 Hz frequency for 30 cycles, unless specified otherwise, for better comparison of different cases.

It is seen from Figures 3.5 (a), (b), and (d) that the time constant or demagnetization decreases with tape thickness, tape width, and number of tapes in a stack, respectively, and (c) shows that demagnetization increases with cross field frequency.

The results are for constant  $J_c$ , and the thickness dependence is in

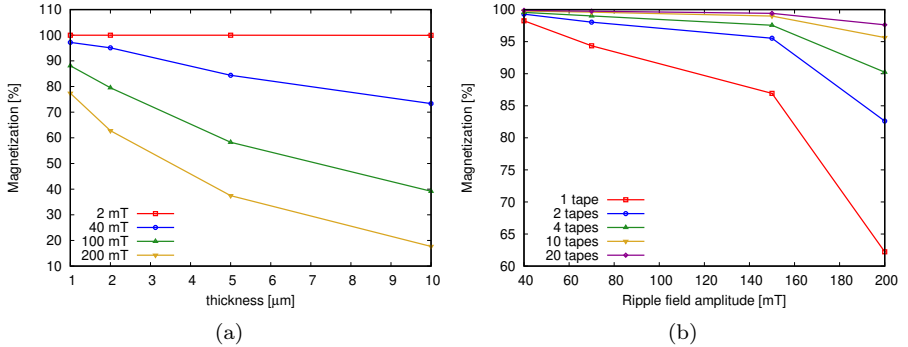


Figure 3.4: Dependence of demagnetization on (a) tape thickness and cross field amplitude (constant  $J_c d$ ), and (b) number of tapes in a stack.

contrast to the result from constant  $J_c d$  case. These trends are due to the dependence of time constant on these state parameters, as can be seen in equations (2.1), (2.2), and (2.3).

### Comparison with analytical formulas

For a single tape, the time constant formulas as given in equation (2.1) and Brandt's equation for single tape ([2]) are used, and their comparisons with the numerical data, for frequency dependence, is shown in Figure 3.6 (a). It can be seen from these graphs that the time constant values for numerical analysis are very close to the data from analytical formulas. Thus, in contrast of non-uniform  $\mathbf{J}$  by Brandt, we validate the approximation of uniform  $\mathbf{J}$  in the width of the tape for our formulas. The numerical method takes non-uniform  $\mathbf{J}$  in both the thickness and width of the tape, so the agreement with numerical results approve of our assumptions. The curves for analytical data are, in general, a bit lower than the numerical results, being more pessimistic, and, hence, providing safer values for engineering applications.

Similarly, the time constant comparison between numerical and analytical results for a stack with different number of tapes is also performed, using equation (2.3) for analytical purposes. The graphs for both these results are in a very good agreement with each other, especially for higher values of ripple fields, as can be seen in Figure 3.6 (b). The agreement is

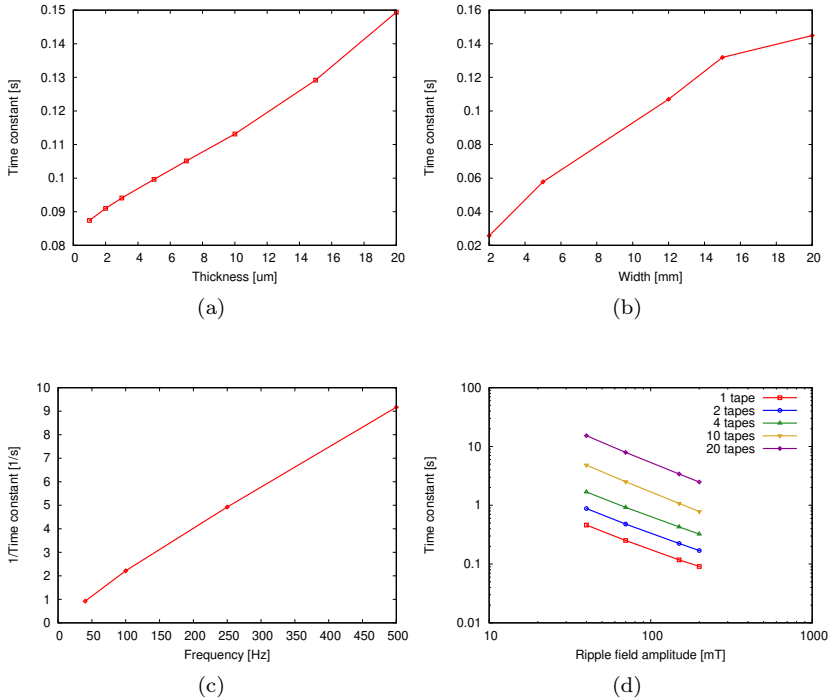


Figure 3.5: Dependence of time constant on (a) tape thickness, (b) tape width, (c) cross field frequency, and (d) number of tapes in stack. The calculations are for constant  $J_c$ .

expected to get better with higher number of computed cycles since these results are calculated at very early stages of demagnetization decay curves. Also, higher Power Law exponent can bring the results closer, since at very high  $n$  values (above 100) the  $E - J$  Power Law Model comes very close to Critical State Model, which the formulas use.

## Dynamic Magneto-Resistance approach

Till now, all the results are achieved by incorporating E-J Power Law in MEMEP method (let's call this E-J Power Law Model). Though the re-

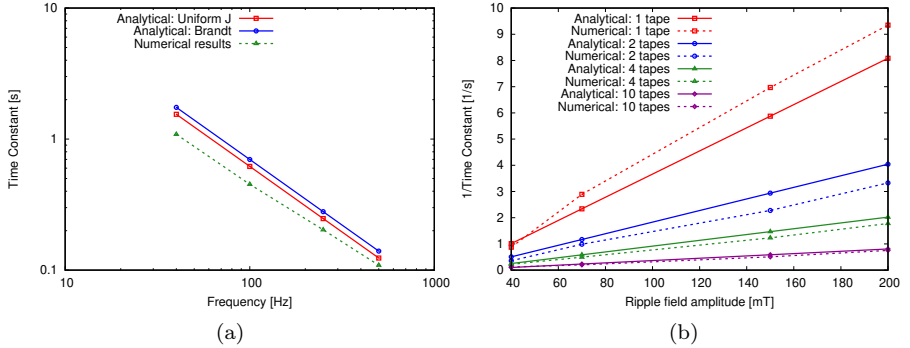


Figure 3.6: Benchmark of analytical formulas for different cases of (a) cross field frequency, and (b) number of tapes dependencies. Numerical calculations agree with simplified formulas for time constant.

sults are accurate, it takes a lot of time to calculate them which depends on various factors such as applied ripple field amplitude, tape/stack geometry, etc. Thus, we use the novel effective E-J relation, developed using Dynamic Magneto-Resistance (DMR model) in MEMEP 2D to calculate demagnetization for millions of cycles of applied cross field.

For this section, we use 2 different configurations for these calculations- Benchmark and Rotor (Table 3.1), according to the different cases.

Modeling configurations		
Parameters	Benchmark	Rotor
Tape Thickness	2 $\mu\text{m}$	1.5 $\mu\text{m}$
Tape Width	12 mm	40 mm
Gap	60 $\mu\text{m}$	100 $\mu\text{m}$
$J_c$	$1.36 \times 10^{10}$ A/m <sup>2</sup>	$5.78 \times 10^{10}$ A/m <sup>2</sup>
Ripple field frequency	500 Hz	2400 Hz

Table 3.1: Different modeling configurations for calculating results with different models.

### Benchmark of DMR model

Firstly, we benchmark DMR model with E-J Power Law model by checking the demagnetization behavior of a 10-tape stack by both models, using Benchmark Configuration, in Figure 3.8. In the (a) part of this Figure, you can see that DMR model shows very good agreement with E-J Power Law model, even for higher number of cycles (100). A little difference (around 0.01 percent) between both models is expected due to the DMR model being based on Critical State Model.

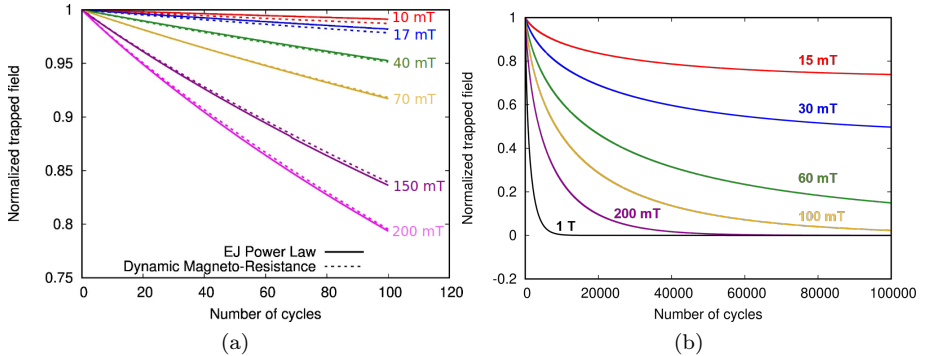


Figure 3.7: Trapped field decay comparison for DMR model, and E-J Power Law Model, using Benchmark configuration for a 10-tape stack (Benchmark configuration). (a) shows good agreement between both models. (b) shows that asymptotic values are reached for ripple field amplitudes below the tape’s penetration field, 55 mT (Rotor configuration).

There are 2 major advantages of DMR model over E-J Power Law model. Firstly, the mesh used in the thickness of tapes in HTS stacks include only one element in DMR model, in contrast to the E-J Power Law model where you need atleast 20 elements in thickness. Secondly, the electric field in DMR model is calculated for one whole cycle (or several cycles) of applied ripple field, whereas, the E-J Power Law model uses 20 time steps in each cycle. Thanks to these benefits, you can calculate demagnetization for very high number of cycles using DMR model fairly quickly. For benchmarking, E-J Power Law model takes 1-2 months for calculating 100 cycles for a 10 tape stack, depending on the applied ripple field amplitude (more time for low amplitudes). For the same case, DMR model takes only around 2 minutes to calculate 100 cycles of demagne-

tization which shows that the DMR model is very strong and fast when compared to its contemporary.

Using these advantages of DMR model, we apply it to calculate demagnetization for 100 thousand cycles of ripple field for a 10-tape stack, this time using Rotor configuration. An interesting result can be seen in Figure 3.8(d) that the trapped field curves at low amplitudes do not decay towards full demagnetization but tend to reach an asymptotic value, whereas the curves at higher amplitude demagnetize to almost zero. This behavior is due to the fact that the dynamic magneto-resistance, which is the cause of demagnetization, is dependent on the tape's threshold field. After some cycles, for low amplitudes, this threshold field becomes relatively very high, in comparison to the ripple field amplitude, that makes the dynamic magneto-resistance practically zero. Hence, there is almost no demagnetization at this point and we see permanent asymptotic values, which means that the tape can stay magnetized at these values practically indefinitely. For high ripple field amplitudes over penetration field, threshold field can never overcome the field amplitude, and the dynamic magneto-resistance cannot reach zero, which makes the tape/stack fully demagnetized.

Here, the tape's parallel penetration field is around 55 mT. So from this we deduce that, if the applied ripple field amplitude is below the tape's penetration field, we get asymptotic or permanent values of trapped field, whereas, if the applied ripple field amplitude is above the parallel penetration field then the sample tends to fully demagnetize.

## Demagnetization of 100 tape stack for millions of cycles

Now, since we have shown that the DMR model is accurate and can present asymptotic values at high number of cycles, we apply the model to a 100 tape stack for high number of applied ripple field cycles. Rotor configuration is used in this section. In real life applications, such as superconducting motors for aircraft, generally 50 to 100 tape thick stacks are used in the rotor, and, thus, modeling such thick stacks is required.

Firstly, the current density profiles for the 100 tape stack can be seen in Figure 3.8 (a) and (b). In order to observe asymptotic values, 30 mT ripple field amplitude is considered for these graphs, as it is below the penetration field of the tape (around 55 mT). The current density profile after relaxation in (a) shows a completely saturated, and uniform stack.

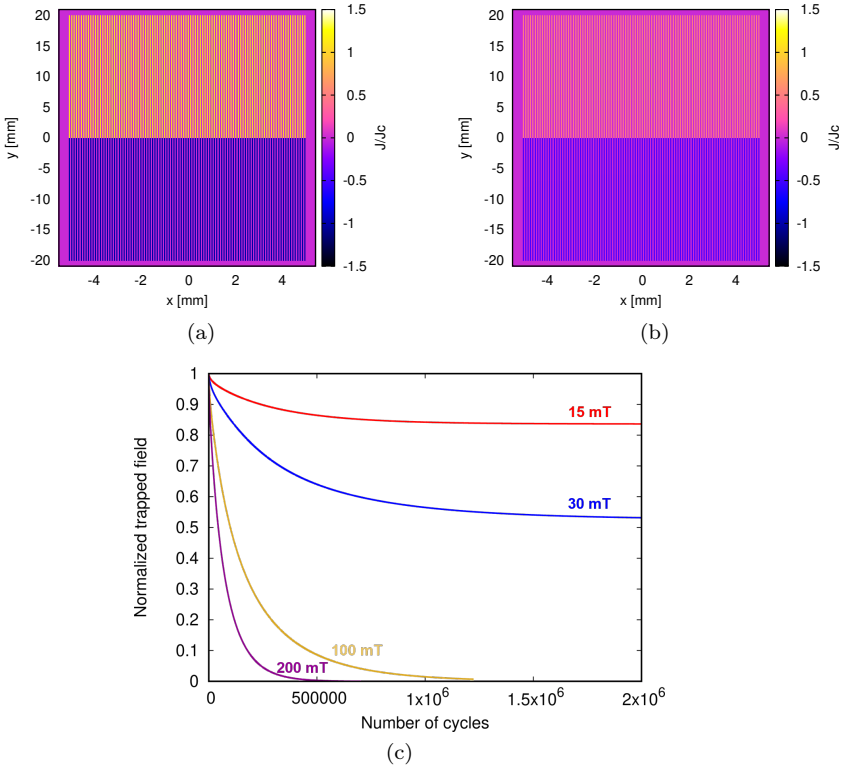


Figure 3.8: Current density profile for 100 tape stack using Rotor configuration at (a) post-relaxation, (b) 100 thousand cycles, and (c) 2 million cycles. Ripple field amplitude applied here is 30 mT.

From (b), it can be seen that even after applying ripple field for 2 million cycles, the stack is not fully demagnetized (where the current density is still around 50 percent of  $J_c$ ), and, hence, a permanent magnetization is retained. Also, the change is not visible here in the thickness of the stack as we only use 1 element in the thickness of the tape. However, the non-uniformity of the current density can be observed in the width of the sample.

In Figure 3.8 (c), we notice that the curves for 15 mT and 30 mT applied ripple field amplitudes reach an asymptotic value, whereas, the other curves demagnetize fully in less than 1 million cycles. Here, we

again show that if the ripple field amplitude is below parallel penetration field of a tape, then the trapped field reaches an asymptotic value and some magnetization is retained permanently. The time taken for calculating 2 million cycles of demagnetization of the 100 tape stack is around 2-4 days, depending on field amplitude, which again shows that the DMR model is very fast when compared to commercial software and E-J Power Law model.

## Other configurations

### HTS Bulks

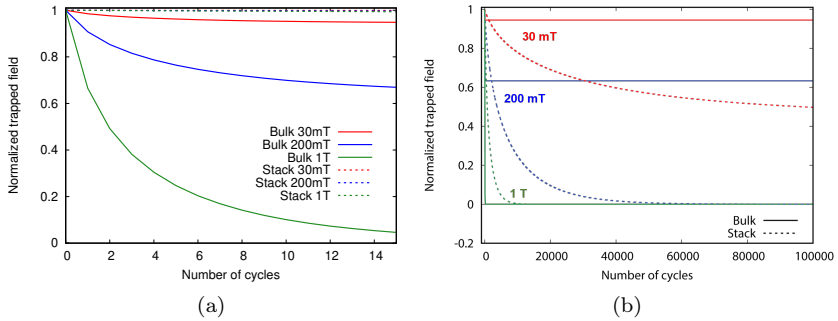


Figure 3.9: Comparison of bulk and stack for (a) low number of cycles, and (b) high number of cycles.

Next, the DMR model is applied to an interesting case of bulks, to compare their demagnetization with stacks for high number of cycles. For this purpose, a 10 tape stack under Rotor configuration parameters is used. Equivalent bulk dimensions of the stack, and engineering critical current density is used for the bulk.

From Figure 3.9, a very striking contrast between the behaviors of bulks and stacks can be observed. We see that for low number of cycles, stacks demagnetize less, whereas, for high number of cycles, bulks demagnetize less. This is due to the fact that bulks have much higher parallel penetration field as compared to the stacks, so bulks have much higher range of ripple field amplitudes for which they can reach an asymptotic

value. In other words, bulks can retain magnetization permanently for ripple field amplitudes higher than the stack's penetration field, and for these fields, stacks get fully demagnetized.

### Soldered stacks

Though we know now that bulks can retain more magnetization than stacks, an important point to note is that constructing a bulk is more complicated than building a stack. Also, stacks are more customizable than bulk. Thus, a good alternative for using bulk for the cross field demagnetization problem can be a fully soldered stack, which acts like a bulk at low resistances [19], in order to have the best of both cases.

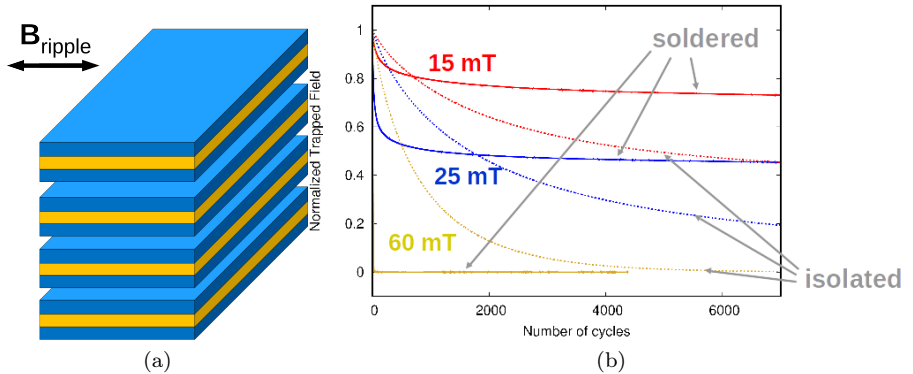


Figure 3.10: (a) Considered configuration 8 tape stack, 4 pairs of soldered stack. (b) Comparison of trapped field curves of 8-tape soldered stacks and isolated stacks.

For this case, we fully solder 2 tapes on the superconducting side. For modeling, we have assumed that all coupling current flows at the end resistance (or the soldering is only at the edges) [19]. Next, we calculate the demagnetization of a stack of a unique construction, where the soldered tapes are arranged in 4 pairs to give a 8-tape soldered-isolated stack, as seen in Figure 3.10 (a).

The demagnetization curves of the soldered stacks and the isolated stacks are calculated using E-J Power Law model and DMR model respectively. Due to higher penetration fields, the soldered stacks also reach

permanent asymptotic fields for cross field amplitudes below their penetration field (48 mT), as can be seen in Fig. 3.10 (b). For 60 mT, both stacks demagnetize to zero since the cross field amplitude is above both of their respective penetration fields. This comparative behavior is the same as the one for the bulk's case in previous section. Thus, we show here that the soldered stacks behave as bulk, and, to avoid rapid demagnetization like isolated stacks, soldered stacks can be used in concerned applications.

# Chapter 4

## Coupled Electro-Magnetic and Electro-Thermal model

We have developed a novel and fast software in C++ which performs coupled Electro-Magnetic (EM) and Electro-Thermal (ET) analysis of superconductors. In the initial stages of development, we have applied this program to the problem of electro-thermal quench, as a proof-of-concept.

For this analysis, a square superconductor sample of dimensions  $1\text{ cm} \times 1\text{ cm}$  is considered. The boiling point or temperature of liquid Nitrogen is taken as  $77\text{ K}$ . The critical temperature ( $T_c$ ) and the critical current density ( $J_c$ ) of the superconductor are taken as  $92\text{ K}$  and  $1 \times 10^8\text{ A/m}^2$ , which are in the range of typical characteristic values of REBCO bulk superconductors. This  $J_c$  is also considered as the critical current density at  $77\text{ K}$ ,  $J_{c,N}$ , and is used to normalize current density profiles in this chapter. The thermal conductivity ( $k$ ) and the thermal heat capacity at constant volume ( $C_v$ ) of the superconductor are taken as  $9\text{ W/m.K}$  and  $9 \times 10^5\text{ J/m}^3/\text{K}$ , respectively, for REBCO superconductor [18, 20]. A physical effective thermal conductivity,  $k_N$ , is considered at the surfaces using convection coefficient,  $h$ , of  $10000\text{ W/m}^2\text{K}$ . The normal state resistivity and Power-Law exponent( $n$ ) are taken as  $3 \times 10^{-7}\text{ }\Omega\text{m}$  and  $30$ , respectively. An important point to note here is that  $n$  and  $C_v$  are temperature dependant, which the software is capable of considering, and the constant values are only taken here for the sake of simplicity. Additionally, the sinusoidal input voltages and magnetic fields are applied at  $50\text{ Hz}$  frequency, with  $20$  time steps per cycle.

## Quench modeling with voltage input

In this section, the quench modeling for the considered superconductor is done using only voltage as an input parameter, where the applied magnetic field is zero. The EM and ET models are coupled with each other, so that for each time step  $J$  from the EM is transferred to the ET, and  $T$  from the ET is transferred to the EM.

The quenching of the magnet is a serious problem, and highly effective cooling conditions and methods are required to overcome this potentially destructive phase. Figure 4.1 (a) and (c) show the rise in average temper-

ature for voltage inputs 1 V/m and 5 V/m, respectively. For 1 V/m, the temperature rise is not big, which is easily overcome by enabling cooling at the surfaces. The low temperatures also do not affect the total current in the sample, and, thus, the total current stays almost the same for the cooling enabled case as well (Figure 4.1 (b)). Contrastingly, for 5 V/m, the average temperature rises very rapidly to above 300 K in just 250 cycles for the adiabatic case. However, with heat exchange with liquid Nitrogen in the cooling enabled case, the average temperature is limited to only around 100 K (just a bit higher than the critical temperature, 92 K), as can be seen in Figure 4.1 (c). This also affects the total current in the sample, and as observed in Figure 4.1 (d), much higher total current is retained for the cooling enabled case. This is because of smaller decrease of  $J_c$  in cooling enabled case, as compared to the adiabatic case, which allows for higher retention of superconducting currents.

Similarly, we analyze various curves of average temperature for different voltage inputs in Figure 4.2. Here, we can see almost no change for voltages 1 V/m and 2 V/m due to effective cooling. For cooling enabled case for 1 V/m, the temperature and current density profiles are presented in Figures 4.3 (a) and (b), respectively. The curves for 10 V/m and 20 V/m amplitudes are for highly limiting case and, with cooling enabled, they reach a stationary state.

The case of 5 V/m with enabled cooling is of special interest, as it still shows relatively high total current (around 3000 A in Figure 4.1(d)), even though the corresponding transient state of average temperature (around 100 K) is above the critical temperature, 92 K (Figure 4.1 (c) ). This effect can be understood by observing the current density and temperature profiles in Figures 4.3 (c) and (d). On letting the program run for 250 cycles, we see that the center of the sample has much higher temperature (around 110 K) than the critical temperature (92 K), which shows that the center of sample is in the normal state (Figure 4.3 (c)). Interestingly, the edges, and some elements near the edges, show temperatures below the critical temperature. Similarly, as can be seen in Figure 4.3 (d), the edges, and some elements extending from the edges, show high current densities in the range of  $J_c$ . This explains the obtained total current curve in Figure 4.1(d), as most of the sample is behaving as a normal conductor but the edges present superconducting behavior, enabling high transfer of currents, given the non-linear nature of superconductors. This shows another feature of using an effective cooling mechanism, that even after achieving normal state at high voltages, a good amount of current can be transmitted using a superconductor in a potent cryogenic environment.

## Quench modeling with applied field input

The coupled Electro-Magnetic and Electro-Thermal model is also able to take applied magnetic field as an input. For this case, we have used input voltage as zero and cooling is enabled. The sinusoidal magnetic field is applied in  $y$  direction (Figure 4.5).

Firstly, we see the average temperature curves for different applied magnetic field inputs in Figure 4.4. For the applied field of 200 mT, the maximum temperature rise from 77 K is quite small and stable during the whole process. There is higher temperature rise for 500 mT. A cyclical rise in temperature is seen for 1 T and 2 T applied field, which is due to cyclic AC power loss generation. An important point to note here is that the total current for the sample will be zero in all these cases, due to the symmetrical nature of current density penetration, which is in contrast to the case of using voltage as an input parameter in the previous section.

Next, the temperature and current density profiles for 500 mT input are analyzed. Figures 4.5 (a) and (b) show, that in just 1 time step, the screening currents start penetrating from the edges inwards. Their sign follows the right-hand rule in order to generate a high magnetic field in the  $y$  direction at the sample center. The temperature change is negligible at this stage. On reducing the applied magnetic field to zero when reaching half cycle, the penetrating screening currents switch their sign (Figures 4.5 (c) and (d)). This effect can be understood from the Critical State Model. Due to this penetration, there appears local heat generation, and, hence, the temperature of the sample rises more.

To note an observable change in the current density profiles due to the temperature rise, the simulation is let to run for up to 150 cycles of applied field. At the end of 150 cycles, we see higher temperatures and lower current densities at the center (Figures 4.5 (e) and (f)). At higher magnetic field inputs, the underlying mechanics of the screening current penetration and temperature rise stays the same, only the rate of the temperature rise increases.

Thus, we show here that the coupled EM and ET model can accurately take the applied magnetic field as input as well, in addition to the voltage as an input parameter, and is able to explain the underlying physics of current and temperature change adequately.

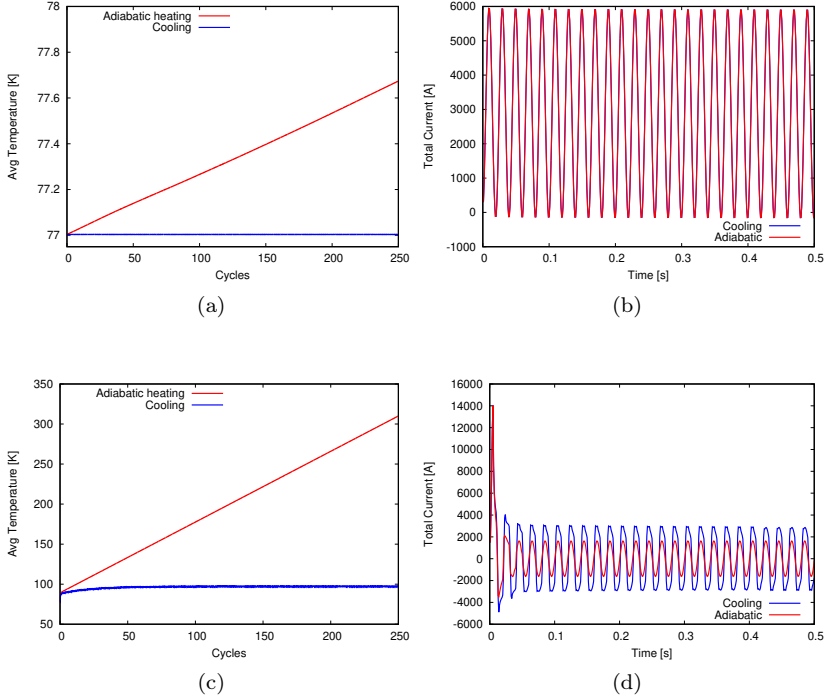


Figure 4.1: Average Temperature and Total current comparison for Adiabatic case and Cooling enabled case respectively taking  $V_m$  as (a,b) 1 V/m, and (c,d) 5 V/m, respectively. At high applied voltages, the superconductor quenches faster, which reduces the total current in the sample rapidly.

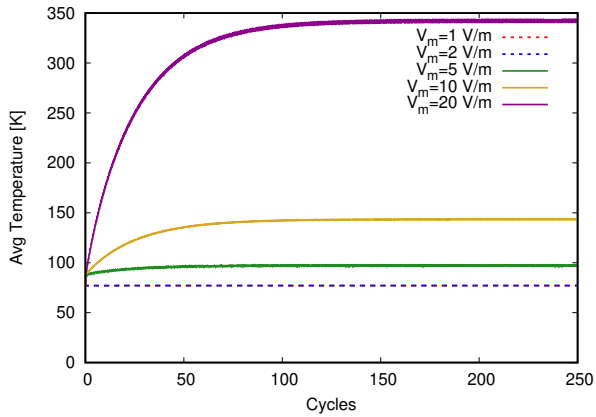


Figure 4.2: Average Temperature curves for different input voltages.

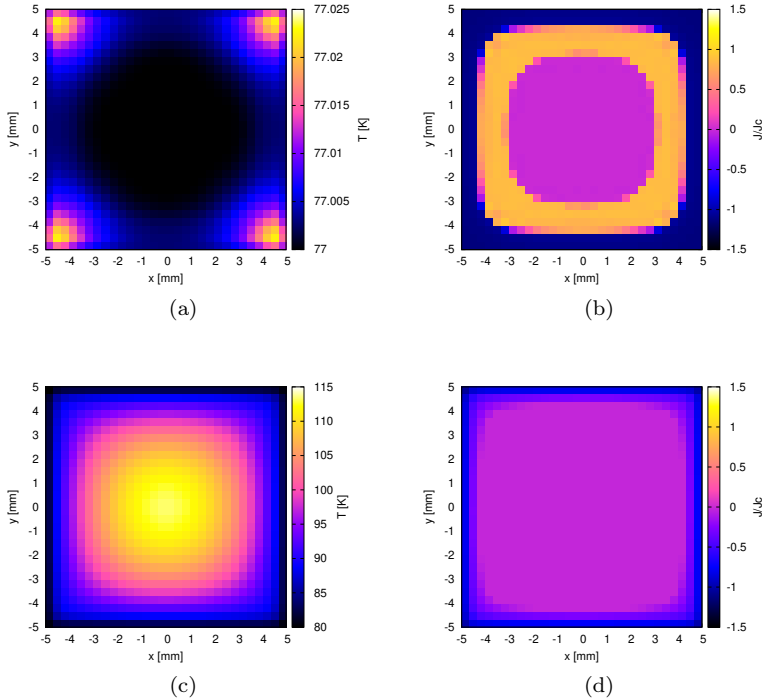


Figure 4.3: Temperature (a,c) and Current Density (b,d) profiles for the cooling enabled case, at the 250th cycle, taking  $V_m$  as (a,b) 1 V/m, and (c,d) 5 V/m, respectively.

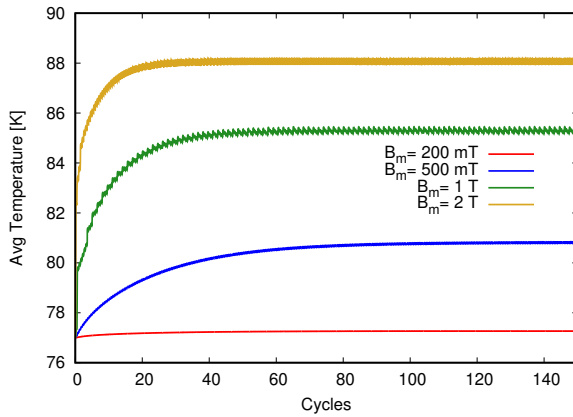


Figure 4.4: Average temperature curves for different applied magnetic field as input. The program is also able to take applied magnetic field as an independent input.

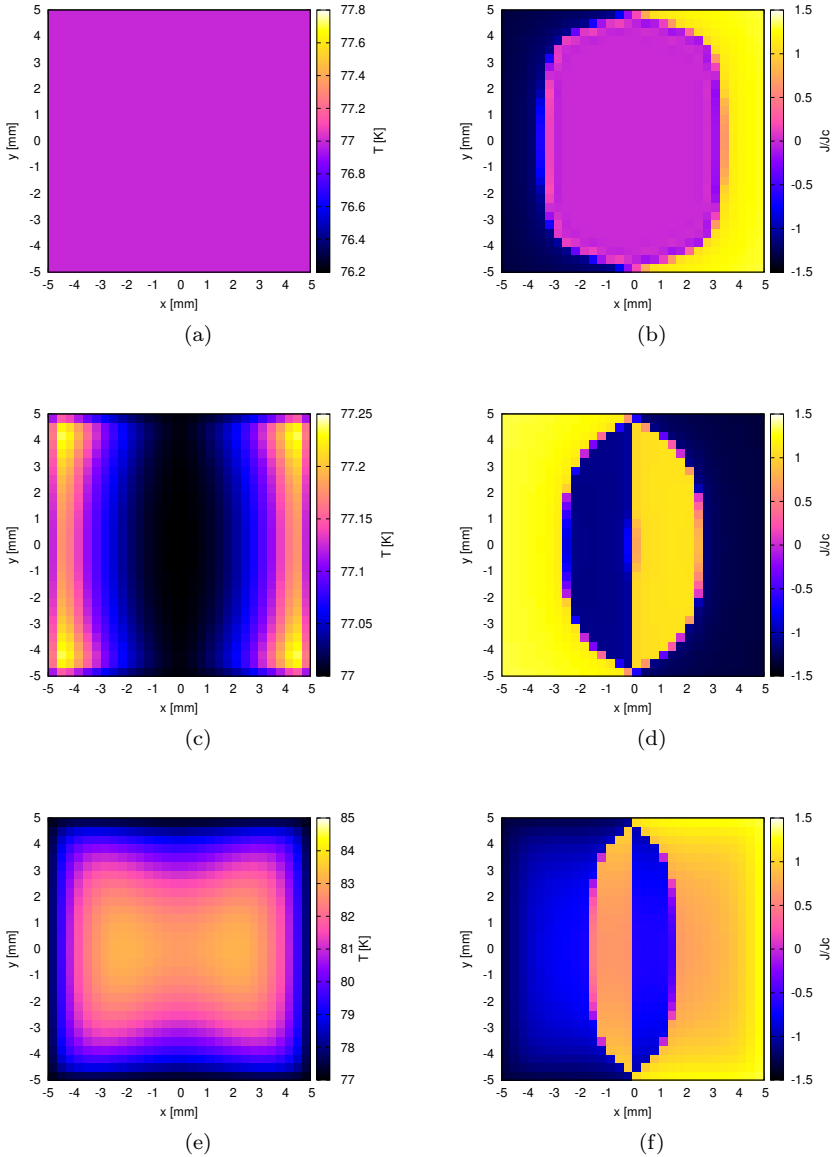


Figure 4.5: Temperature (a,c,e) and Current Density (b,d,f) profiles for applied field,  $B_m$ , of 500 mT, cooling enabled case, at the (a,b) 1st time step ( $B_a/B_m = 0.2$ ) of the 1st cycle, (c,d) the half cycle (applied field  $B_a = 0$ ) of the 1st cycle, and (e,f) at the 150th cycle, respectively.

# Chapter 5

## Conclusion

### Cross field demagnetization of HTS stacks and bulks

We show that the 2D MEMEP model, using E-J Power Law (called E-J Power Law Model), is able to model the phenomenon of cross field demagnetization of HTS stacks and bulks accurately. The 2D model is benchmarked with 3D model, and we see that the trapped fields at the center of tape lengths of 3 times the width (3D MEMEP) is practically the same as for the infinitely long tapes (2D MEMEP). We use the 2D MEMEP model to calculate the time constant of the deteriorating curve of the stack's trapped field, a measure of magnetization decay rate, and we see that the numerical results for the time constant also agree with the analytical formulas' results developed by our team.

It is found that the demagnetization of a superconducting tape, or stack of tapes, is dependent on various state variables like applied ripple magnetic field amplitude and frequency, thickness and width of the tape, and number of tapes in stacks. The time constant increases with tape thickness (constant  $J_c$ ), tape width, and number of tapes in stack, and decreases with in ripple field amplitude and frequency. The demagnetization also increases with thickness of tape for critical sheet current density (constant  $J_c d$ ).

We also develop a novel effective E-J relation, based on Dynamic Magneto-Resistance (we call this DMR model), which is used to calculate the demagnetization of a 100-tape stack for over 2 million cycles of ripple field in less than 4 days, which is the current world record, as per our knowledge. From this calculation, we see that if the applied ripple field amplitude is below the parallel penetration field of the tape, then the trapped field curves reach an asymptotic value, where we achieve permanent magnetization for indefinite time. For ripple field amplitudes above the parallel penetration field of the tape, the stack fully demagnetizes. We apply this model to other interesting cases as well, such as bulks and soldered stacks, and show that they retain more magnetization for high number of cycles as their parallel penetration fields are much higher than isolated stacks.

The frequencies in HTS motors for aviation are very high (1000s of Hz), thus, we need to calculate demagnetization of HTS stacks for millions of cycles to account for the real flight times, which are atleast 2 hours for

transcontinental flights. The DMR model developed during this thesis can, thereby, assist the motor engineers to effectively design superconducting motors, enabling them in the pursuit of realtime and fast calculation of the cross field demagnetization of HTS stacks and bulks.

### **Coupled Electro-Thermal modeling of superconductors**

We have also developed a novel computer software which performs coupled 2D Electro-Thermal (ET) and Electro-Magnetic (EM) analysis of superconductors. The ET and EM codes work in conjunction, and affect each other, for every timestep, and are based on Minimum Electro-Thermal Entropy Production (METEP) and Minimum Electro-Magnetic Entropy Production (MEMEP), respectively.

The software is able to accurately and quickly predict the magnetic quench behavior using different inputs, and can explain the physics of temperature and current density change in detail. The models are programmed in C++ at our department, and, thus, they are highly customizable to take more inputs and variables, and include other physical analyses as well. The software, built using completely new methods, is currently in the initial development phase, and shows great promise for the complete multiphysical analysis of superconductors for different high field and power applications.

For future work, for coupled Electro-Thermal and Electro-Magnetic model, we plan to upgrade the software by including temperature dependence of different variables, like  $C_v(T)$ ,  $n(T)$ , and  $k(T)$ . Then, the software will be applied to the geometry of axisymmetric coil, for Electro-Thermal and Electro-Magnetic analyses. It is also planned to add coupled Mechanical analysis by the end of this year (2021) in the C++ program, which will enable us to completely analyze the multiphysics of superconductors for high field magnets under the Hi-SCALE project.

# Publications and Conferences

## Publications

- **Dadhich, A.** and Pardo, E.: Modeling cross-field demagnetization of superconducting stacks and bulks for up to 100 tapes and 2 million cycles, Scientific Repoerts, 10(1), pp.1-11, 19265, 2021. (IF 3.998)
- **Dadhich, A.**, Pardo, E., and Kapolka, M.: Time constant of the transverse-field demagnetization of superconducting stacks of tapes, Superconductor Science and Technology, 33(6) 065003, 2020. (IF 3.067)
- Kapolka, M., Pardo, E., Grilli, F., Baskys, A., Climente-Alarcon, V., **Dadhich, A.**, and Glowacki, B.A.: Cross-field demagnetization of stacks of tapes: 3D modeling and measurements, Superconductor Science and Technology, 33(4), 044019, 2020. (IF 3.067)
- Grilli, F., Benkel, T., Hänisch, J., Lao, M., Reis, T., Berberich, E., Wolfstädter, S., Schneider, C., Miller, P., Palmer, C., Glowacki, B., Climente-Alarcon, V., Smara, A., Tomkow, L., Teigelkötter, J., Stock, A., Büdel, J., Jeunesse, L., Staempflin, M., Delautre, G., Zimmermann, B., van der Woude, R., Perez, A., Samoilenkov, S., Molodyk, A., Pardo, E., Kapolka, M., Li, S., and **Dadhich, A.**: Superconducting motors for aircraft propulsion: the Advanced Superconducting Motor Experimental Demonstrator project, Journal of Physics: Conference Series, 1590(1) 012051, 2020.

## Conferences

Underlined are the presenting authors.

- Dadhich, A., Pardo, E., Solovyov, M., Li, S., Mosat, M., Souc, J.: Reducing cross-field demagnetization in stacks of REBCO tapes by soldering, Materials Research Society (MRS) 2021, Virtual Conference, USA. (Oral)
- Dadhich, A. and Pardo, E.: Modeling the cross field demagnetization of REBCO stacks and bulks for millions of cycles. In Applied Superconductivity Conference (ASC) 2020, Virtual Conference, USA. (Student Paper Competition - Oral)
- Dadhich, A., Kapolka, M., Pardo, E., Climente-Alarcon, V., Smara, A., Mineev, N., Tomkow, L., Glowacki, B.A., and Grilli, F.: Cross-field demagnetization of 2G HTS stacks for high number of cycles. 14<sup>th</sup> European Conference on Applied Superconductivity (EUCAS) 2019, Glasgow, Scotland. (Oral)
- Pardo, E., Dadhich, A., Li, S., Kapolka, M., Solovyov, M., Mošaf, M., Kováč, J., and Šouc, J.: Modeling and measuring the cross field demagnetization of REBCO stacks and bulks for millions of cycles. Applied Superconductivity Conference (ASC) 2020, Virtual Conference, USA. (Invited Talk)
- Grilli, F., Benkel, T., Hänisch, J., Reis, T., Berberich, E., Wolfstädter, S., Schneider, C., Miller, P., Palmer, C., Glowacki, B., Climente-Alarcon, V., Smara, A., Tomkow, L., Teigelkötter, J., Stock, A., Büdel, J., Jeunesse, L., Staempfli, M., Delautre, G., Zimmermann, B., van der Woude, R., Perez, A., Samoilenkov, S., Molodyk, A., Pardo, E., Kapolka, M., Li, S., and Dadhich, A.: REBCO coated conductors are ready to take off. SuperFOx 2020, Santa Margherita Ligure, Italy. (Invited Talk)

# Bibliography

- [1] Oswald Elektromotoren GmBh, “ASuMED - Advanced Superconducting Motor Experimental Demonstrator,” *H2020 Project*, 2017, [www.asumed.oswald.de](http://www.asumed.oswald.de).
- [2] E. Brandt and G. Mikitik, “Why an AC Magnetic Field Shifts the Irreversibility Line in Type-II Superconductors,” *Physical Review Letters*, vol. 89, no. 2, 2002.
- [3] M. Baghdadi, H. S. Ruiz, and T. A. Coombs, “Crossed-magnetic-field experiments on stacked second generation superconducting tapes: Reduction of the demagnetizing effects,” *Applied Physics Letters*, vol. 104, p. 232602, 2018.
- [4] A. M. Campbell, M. Baghdadi, A. Patel, D. Zhou, K. Y. Huang, Y. Shi, and T. Coombs, “Demagnetisation by crossed fields in superconductors,” *SuST*, vol. 30, no. 3, p. 034005, 2017.
- [5] F. Liang, T. Qu, Z. Zhang, J. Sheng, W. Yuan, Y. Iwasa, and M. Zhang, “Vortex shaking study of REBCO tape with consideration of anisotropic characteristics,” *Supercond. Sci. Technol.*, vol. 30(9), p. 094006, 2017.
- [6] M. Baghdadi, H. S. Ruiz, and T. A. Coombs, “Nature of the low magnetization decay on stacks of second generation superconducting tapes under crossed and rotating magnetic field experiments,” *Scientific Reports*, vol. 8(1), p. 1342, 2018.
- [7] A. Smara, N. Mineev, V. Climente-Alarcon, A. Patel, A. Baskys, B. A. Glowacki, and T. Reis, “An experimental assessment of rotor superconducting stack demagnetization in a liquid nitrogen environment,” *Superconducting Science and Technology*, vol. 32, p. 085009, 2019.
- [8] A. Baskys, A. Patel, and B. Glowacki, “Measurements of crossed-field demagnetization rate of trapped field magnets at high frequencies and below 77k,” *Supercond. Sci. Technology*, vol. 31, 2018.
- [9] P. Vanderbemden, Z. Hong, T. Coombs, M. Ausloos, N. Hari Babu, D. Cardwell, and A. Campbell, “Remagnetization of bulk high-temperature superconductors subjected to crossed and rotating magnetic fields,” *Supercond. Sci. Technol.*, vol. 20, p. S174, 2007.
- [10] D. Zhou, M. Izumi, M. Miki, B. Felder, T. Ida, and M. Kitano, “An overview of rotating machine systems with high-temperature bulk superconductors,” vol. 25, no. 10, p. 103001, 2012.

- [11] J. Srpcic, F. Perez, Y. Huang, K. Y. and Shi, M. D. Ainslie, A. R. Dennis, M. Filipenko, M. Boll, D. A. Cardwell, and J. H. Durrell, "Penetration depth of shielding currents due to crossed magnetic fields in bulk RE-Ba-Cu-O superconductors," *Superconducting Science and Technology*, vol. 32, p. 035010, 2019.
- [12] J. Srpcic, D. Zhou, K. Huang, Y. Shi, A. Dennis, M. D. Ainslie, A. M. Campbell, R. Bause, M. Boll, M. Filipenko, D. A. Cardwell, and J. H. Durrell, "Demagnetization study of pulse-field magnetized bulk superconductors," vol. 28, p. 6801305, 2018.
- [13] J. Schwartz, "Quench in high temperature superconductor magnets," in *WAMSDO: Workshop on Accelerator Magnet Superconductors, Design and Optimization*, 2013, p. 21.
- [14] R. Bellis and Y. Iwasa, "Quench propagation in high tc superconductors," *Cryogenics*, vol. 34, no. 2, pp. 129–144, 1994.
- [15] E. Pardo, J. Šouc, and L. Frolek, "Electromagnetic modelling of superconductors with a smooth current-voltage relation: variational principle and coils from a few turns to large magnets," vol. 28, p. 044003, 2015.
- [16] M. Kapolka, J. Srpcic, D. Zhou, M. Ainslie, E. Pardo, and A. Dennis, "Demagnetization of cubic Gd-Ba-Cu-O bulk superconductor by cross-fields: measurements and 3D modelling," vol. 28, p. 6801405, 2018.
- [17] E. Pardo, "Modeling of screening currents in coated conductor magnets containing up to 40000 turns," *Supercond. Sci. Technol.*, vol. 29(8), 2016, 085004.
- [18] F. Roy, B. Dutoit, F. Grilli, and F. Sirois, "Magneto-thermal modeling of second-generation HTS for resistive fault current limiter design purposes," *IEEE transactions on applied superconductivity*, vol. 18, no. 1, pp. 29–35, 2008.
- [19] S. Li and E. Pardo, "Resistance Dependence of the Magnetization Loss for the Partially Coupled REBCO Stacks Modeled by MEMEP Method," in *2020 IEEE International Conference on Applied Superconductivity and Electromagnetic Devices (ASEMD)*, 2020, pp. 1–2.
- [20] F. Roy, "Modeling and characterization of coated conductors applied to the design of superconducting fault current limiters- thesis," EPFL, Tech. Rep., 2010.